

## Simulated long-term changes in river discharge and soil moisture due to global warming

SYUKURO MANABE<sup>1</sup>, P. C. D. MILLY<sup>2</sup> &  
RICHARD WETHERALD<sup>3</sup>

<sup>1</sup> Program in Atmospheric and Oceanic Sciences, Princeton University, PO Box CN710, Princeton, New Jersey 08544-0710, USA

[manabe@splash.princeton.edu](mailto:manabe@splash.princeton.edu)

<sup>2</sup> US Geological Survey, Geophysical Fluid Dynamics Laboratory/ NOAA, PO Box 308, Princeton, New Jersey 08542-0308, USA

[cmilly@usgs.gov](mailto:cmilly@usgs.gov)

<sup>3</sup> Geophysical Fluid Dynamics Laboratory/ NOAA, PO Box 308, Princeton, New Jersey 08542-0308, USA

[dick.wetherald@noaa.gov](mailto:dick.wetherald@noaa.gov)

**Abstract** By use of a coupled ocean–atmosphere–land model, this study explores the changes of water availability, as measured by river discharge and soil moisture, that could occur by the middle of the 21st century in response to combined increases of greenhouse gases and sulphate aerosols based upon the “IS92a” scenario. In addition, it presents the simulated change in water availability that might be realized in a few centuries in response to a quadrupling of CO<sub>2</sub> concentration in the atmosphere. Averaging the results over extended periods, the radiatively forced changes, which are very similar between the two sets of experiments, were successfully extracted. The analysis indicates that the discharges from Arctic rivers such as the Mackenzie and Ob’ increase by up to 20% (of the pre-Industrial Period level) by the middle of the 21st century and by up to 40% or more in a few centuries. In the tropics, the discharges from the Amazonas and Ganga-Brahmaputra rivers increase substantially. However, the percentage changes in runoff from other tropical and many mid-latitude rivers are smaller, with both positive and negative signs. For soil moisture, the results of this study indicate reductions during much of the year in many semiarid regions of the world, such as the southwestern region of North America, the northeastern region of China, the Mediterranean coast of Europe, and the grasslands of Australia and Africa. As a percentage, the reduction is particularly large during the dry season. From middle to high latitudes of the Northern Hemisphere, soil moisture decreases in summer but increases in winter.

**Key words** coupled model; global climate change; global warming; potential evaporation; precipitation; river discharge; soil moisture; water availability

### Simulations à long terme de changements d’écoulement fluvial et d’humidité du sol causés par le réchauffement global

**Résumé** Cette étude explore, grâce à un modèle couplé océan–atmosphère–continents, les changements dans la disponibilité en eau, traduite par l’écoulement fluvial et l’humidité du sol, qui pourraient apparaître au milieu du 21<sup>ème</sup> siècle; en réponse aux augmentations combinées des gaz à effet de serre et des aérosols sulfatés du scénario “IS92a”. Elle présente, en outre, la simulation du changement dans la disponibilité en eau qui pourrait apparaître dans quelques siècles, suite à un quadruplement de la concentration en CO<sub>2</sub> dans l’atmosphère. En moyennant les résultats sur les périodes étendues, les changements issus des forçages radiatifs, qui se révèlent être très similaires pour les deux expériences, ont été obtenus avec succès. L’analyse indique que les écoulements produits par les fleuves arctiques, comme le Mackenzie et l’Ob’, augmentent de 20% (par rapport au niveau de la période pré-industrielle) au milieu du 21<sup>ème</sup> siècle, et d’au moins 40% dans quelques siècles. Sous les tropiques, les écoulements de l’Amazone et du Gange-Brahmapoutre augmentent de manière substantielle. Cependant, les pourcentages de changement dans l’écoulement sont plus faibles pour d’autres fleuves tropicaux, et pour de nombreux fleuves des latitudes intermédiaires, avec des variations aussi bien positives que négatives. Du point de vue de l’humidité du sol, les résultats de cette étude indiquent des diminutions durant une

grande partie de l'année, dans de nombreuses régions semiarides du monde, comme dans le Sud-Ouest de l'Amérique du Nord, le Nord-Est de la Chine, l'Europe Méditerranéenne, et les prairies d'Australie et d'Afrique. En pourcentage, la diminution est particulièrement importante en période sèche. Sous les latitudes moyennes à hautes de l'Hémisphère Nord, l'humidité du sol diminue en été, mais augmente en hiver.

**Mots clefs** modèle couplé; changement climatique global; évaporation potentielle; précipitation; écoulement fluvial; humidité du sol; disponibilité en eau

## INTRODUCTION

As the concentrations of greenhouse gases (e.g. CO<sub>2</sub>, CH<sub>4</sub> and H<sub>2</sub>O) associated with global warming increase in the atmosphere, the downward flux of infrared radiation increases, thereby making more energy available for evaporation. Thus, evaporation from the Earth's surface is enhanced. The increase in evaporation in turn alters precipitation not only *in situ*, but also in other regions of the world due to the three-dimensional circulation of the atmosphere. In those regions where the precipitation is substantially greater than potential evaporation (total radiative energy available for evaporation), the increase in precipitation often results in an increase in runoff, thereby increasing total river discharge. In contrast, in those regions where precipitation is substantially less than potential evaporation, the increase (reduction) in precipitation does not necessarily enhance (reduce) runoff substantially. Instead, it often induces an increase (reduction) in soil moisture. This is because it is necessary that soil moisture is maintained at an elevated (reduced) level in order to maintain the balance between precipitation and evaporation in the long run.

Based upon the analysis of an ensemble of numerical experiments, Wetherald & Manabe (2002) investigated the change in water availability (i.e. river discharge and soil moisture) simulated for the middle of the 21st century. Averaging the results from an ensemble of eight experiments, they identified some of the systematic changes in water availability that had hitherto been obscured by large, unforced natural variability.

According to Walker & Kasting (1992), Draconian measures would probably be required to prevent the atmospheric CO<sub>2</sub> concentration from quadrupling in a few centuries. This is one of the primary reasons why Milly *et al.* (2002) and Manabe *et al.* (2004) investigated the simulated change in water availability that results from a quadrupling of atmospheric carbon dioxide.

Based upon a comparative assessment of the results obtained from the two preceding studies (Wetherald & Manabe, 2002; Manabe *et al.*, 2004), the present study attempts to identify and discuss systematic changes in the rate of river discharge and soil moisture during the next few centuries.

## COUPLED ATMOSPHERE–OCEAN–LAND MODEL

The model used in this study consists of coupled general circulation models (GCMs) of the atmosphere and oceans and a highly idealized land model that includes budgets of heat and water. This coupled atmosphere–ocean–land model is referred to herein as the “coupled model”. The three components of the model interact through exchanges of heat, water and momentum and are described below.

The atmospheric component of the coupled atmosphere–ocean–land climate model solves the equations of motion on a sphere using the spectral-transform method (Orsag, 1970). Horizontal distributions of variables are represented by truncated series of spherical harmonics and grid point values, with zonal truncation at wave number 30. The corresponding transform grid has a spacing of  $3.75^\circ$  in longitude and  $2.25^\circ$  in latitude. In the vertical direction, there are 14 unevenly spaced levels for finite-difference computation. A seasonally varying insolation is prescribed at the top of the atmosphere. The effects of clouds, water vapour, carbon dioxide and ozone are included in the calculation of solar and terrestrial radiation. Clouds are predicted whenever relative humidity exceeds a critical threshold that varies with height. Precipitation is simulated whenever the predicted water content of air exceeds saturation. The vertical redistribution of temperature and water vapour due to moist convection is represented by a simple scheme called moist convective adjustment (Manabe *et al.*, 1965). A water budget is computed at each continental grid cell for a “bucket” having a globally constant moisture-holding capacity of 15 cm as the difference between the field capacity and the wilting point of soil moisture, integrated over the root zone of the soil (Manabe, 1969). Evaporation is a function of soil moisture and potential evaporation computed assuming a saturated land surface (Milly, 1992). Where the predicted water content of the bucket exceeds the capacity, any excess water is converted to runoff, which is then collected over river basins and transported instantaneously to river mouths at the ocean.

The oceanic component of the coupled model numerically solves the primitive equations of motion. The grid size for the finite-difference computation is  $1.75^\circ$  in longitude by  $2.25^\circ$  in latitude, with 18 unevenly spaced levels in the vertical dimension. Horizontal and vertical mixing of momentum, heat and salt by subgrid-scale eddies is parameterized (Bryan & Lewis, 1979). In addition, the mixing of heat and salt along surfaces of constant density by subgrid-scale eddies is included (Redi, 1982). The coupled model uses a relatively simple thermodynamic model of sea ice, in which sea ice moves with surface ocean currents, unless it is thicker than 4 m and converging, in which case it does not move.

The coupled model used here employs a procedure called flux adjustment (e.g. Manabe *et al.*, 1991). If applied successfully, this technique prevents a systematic drift of surface temperature, salinity and sea ice from realistic values without damping their anomalies. This implies that the anomalous fluxes of heat and water at the ocean–atmosphere interface induce anomalies of surface temperature and salinity. Thus, a coupled model with flux adjustment may be regarded as an “anomaly model”. As the sensitivity of a model climate depends critically upon the distribution of sea-surface temperature, it is very desirable that the sea-surface temperature remains realistic in the absence of thermal forcing. In the authors’ opinion, this technique provided an attractive alternative, pending the construction of a more realistic climate model.

As Figure 1 of Wetherald & Manabe (2002) illustrates, the broad-scale features of the global distribution of annual precipitation are quite realistic, particularly over continents. However, upon further inspection, one notes that the model substantially underestimates precipitation over tropical oceans due probably to the failure of the model to resolve intense tropical storms, which preferentially generate very intense precipitation over the ocean. On the other hand, possibly as a consequence of the oceanic precipitation deficit, the model overestimates precipitation over tropical continents. Consistent with these features of the precipitation simulation, Milly *et al.*

(2002) reported that the model simulates well the annual discharges of major rivers far outside the tropics but, in general, overestimates discharges in the tropics. The coupled model used here has twice as high a resolution as the original version constructed by Manabe *et al.* (1991), and yields an improved simulation of the broad-scale feature of precipitation. For a detailed evaluation of performance of the coupled model in reproducing the observed characteristics of climate, see Delworth *et al.* (2002).

## NUMERICAL EXPERIMENTS

### IS92a experiments

The numerical experiments used in this study comprise an eight-member ensemble of experiments, with radiative forcing by increasing CO<sub>2</sub>-equivalent concentration of greenhouse gases and sulphate aerosols from 1865 to 2090. The members of the ensemble began from different initial conditions, each taken from the control run with spacing of at least 40 years. The radiative forcing is identical to that used by Haywood *et al.* (1997). It was determined using estimates of past and future equivalent carbon dioxide concentration and sulphate loading, and is very similar to the IS92a scenario of the Intergovernmental Panel on Climate Change (IPCC, 1992); thus, it is referred to as “IS92a” herein. For the 21st century, this radiative forcing is in the middle range of the more recent SRES (Special Report on Emission Scenario) compiled by the Intergovernmental Panel on Climate Change (IPCC, 2001).

The time series of global mean surface air temperature and global mean rate of precipitation from the eight IS92a experiments are illustrated in Fig. 1. This figure indicates, in terms of ensemble averages, that global surface air temperature increases by approximately 2.3°C and global mean precipitation increases by 5.2% from the pre-Industrial Period to the middle of the 21st century. The geographical distribution of the change in surface temperature is shown in Fig. 2(a). A change from the pre-Industrial Period to the middle of the 21st century is obtained by subtracting the 900-year mean value of the control experiment from the average over the 30-year period from 2035 to 2065 of the eight climate-change experiments combined, for an effective 240-year sample duration.

### CO<sub>2</sub>-quadrupling experiment

In addition to the IS92a experiments described above, a CO<sub>2</sub>-quadrupling experiment (4×C) was conducted, with atmospheric carbon dioxide increasing at a rate of 1% per year (compounded) until it reaches four times the initial (control) value at the ~140th year and remains unchanged thereafter. (Here, the atmospheric CO<sub>2</sub> may be regarded as the CO<sub>2</sub> equivalent of all greenhouse gases combined.) The influence of anthropogenic aerosols was not considered in this experiment, because it is likely to be relatively less important over century time scales as emission control of sulphur dioxide is strengthened.

By the ~140th year of 4×C, when the atmospheric CO<sub>2</sub> concentration has quadrupled, the global surface air temperature increases by ~5°C, and it increases very slowly thereafter, yielding a warming of ~5.5°C by the 250th year of the experiment.

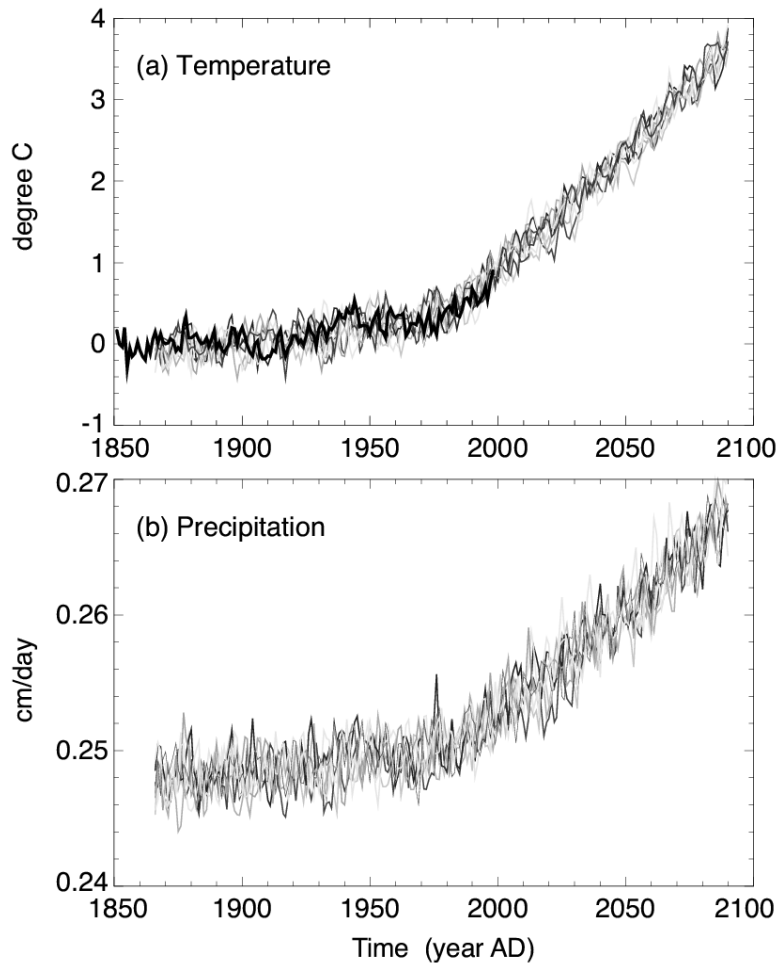


**Fig. 1** Time series of (a) globally averaged, annual mean surface air temperature anomaly ( $^{\circ}\text{C}$ ), and (b) globally averaged, annual mean rate of precipitation ( $\text{cm day}^{-1}$ ), which are obtained from an ensemble of the eight climate-change experiments (IS92a). The thick black line in (a) indicates a time series of observed annual mean, global mean surface air temperature, which was constructed and updated by Jones & Wigley (1991). From Wetherald & Manabe (2002).

Over continents, the warming is between  $5$  and  $10^{\circ}\text{C}$  and is generally larger than over oceans in the middle and high latitudes of the Northern Hemisphere (Fig. 2(b)). To obtain a robust estimate, a change due to quadrupling of atmospheric carbon dioxide is calculated by subtracting the 900-year mean value of the control experiment from the 100-year average between the 200th and 300th years of the  $\text{CO}_2$ -quadrupling experiment. However, the simulated changes of surface temperature and water availability (e.g. river discharge and soil moisture) realized by year 200 are almost as large as the changes averaged from year 200 to year 300.

## RIVER DISCHARGE

Table 1 presents a comparison of historical mean values of annual discharge and model-estimated mean values of annual discharge from the control experiment. In high and middle latitudes about half of the basins have modelled discharges within about

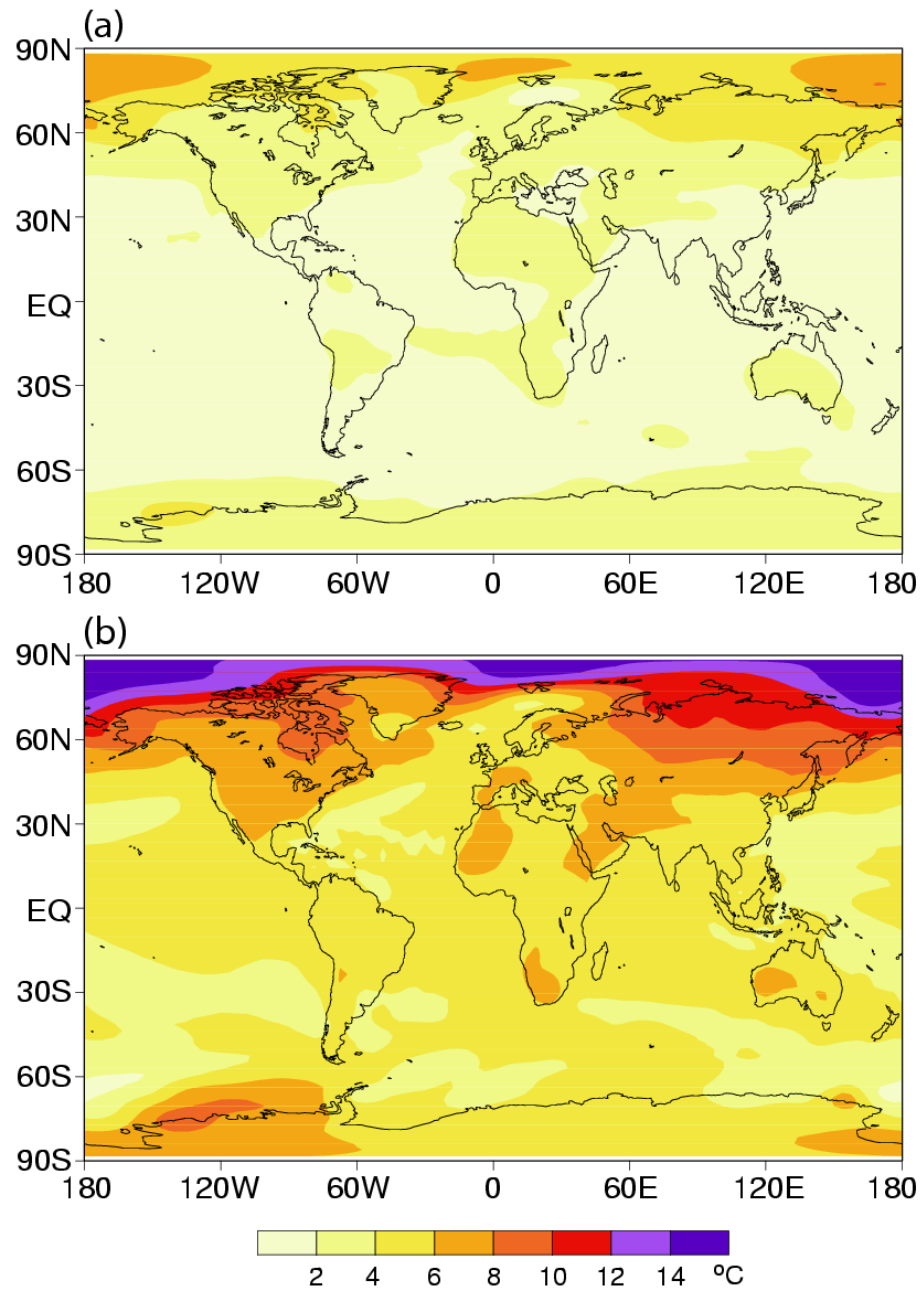


**Fig. 2** Geographical distributions of the change in annual mean surface temperature (°C) simulated to occur: (a) from the pre-Industrial Period to the middle of the 21st century (IS92a); and (b) in response to the quadrupling of atmospheric carbon dioxide. (a) and (b) are taken from Wetherald & Manabe (2002) and Manabe *et al.* (2004), respectively.

20% of observed values. High- and middle-latitude sums of modelled discharge ( $52\,700$  and  $97\,500\text{ m}^3\text{ s}^{-1}$ , respectively) compare reasonably well with observed values ( $63\,200$  and  $84\,400\text{ m}^3\text{ s}^{-1}$ ). In view of the fact that runoff is a relatively small difference between precipitation and evaporation, the simulation of river discharges in middle and high latitudes is considered to be satisfactory.

In the low latitudes, river discharges are generally overestimated. In basins that produce relatively low runoff, the relative errors are especially large. Considering

again the fact that runoff is the residual of precipitation after evapotranspiration is removed, it is not surprising that such large discharge errors would result when precipitation is systematically overestimated over the continents, as already mentioned.

The comparisons of observed and modelled discharge made in this study are affected by temporal sampling errors in the observations, because observational records are not always long enough to provide precise estimates of climatic means. Additionally, the natural balance between runoff and evapotranspiration is modified significantly in some arid regions as a result of irrigated agriculture and evaporation from artificial reservoirs. However, both sampling errors and water-resource development are small compared to the simulation errors in the basins for which comparisons are made in Table 1.

In response to the increase in the CO<sub>2</sub> concentration in the atmosphere, the temperature increases not only at the Earth's surface but also in the troposphere, thereby inducing an increase in the absolute humidity of air. The changes in temperature and concentrations of greenhouse gases (e.g. water vapour as well as carbon dioxide) result in an increase of the net downward flux of infrared radiation, making more energy available for evaporation from the Earth's surface. More evaporation, in turn, results in more precipitation (e.g. Manabe & Wetherald, 1975; Wetherald & Manabe, 1975).

Simulated precipitation and evaporation both increase by 5.2% by the middle of the 21st century and by 12.7% due to the quadrupling of carbon dioxide. The percentage increase in river discharge averaged over all continents is 7.3% by the middle of 21st century, and is 14.8% due to CO<sub>2</sub>-quadrupling.

The geographical distributions of the changes in the rate of runoff simulated for the middle of the 21st century and for the CO<sub>2</sub>-quadrupling are illustrated in Fig. 3(a) and (b), respectively. Although the magnitudes of the changes differ by a factor of about two, the distributions of the changes are remarkably similar. This similarity indicates that this study succeeded in extracting the radiatively forced change from the large natural variability.

The percentage changes in the rates of discharge from major rivers of the world are given in Table 1. As Fig. 3 and Table 1 indicate, the changes are relatively large in high northern latitudes, in qualitative agreement with results from early as well as recent studies (e.g. Manabe & Wetherald, 1985; Arora & Boer, 2001). For example, the rates of simulated discharge from some Arctic rivers, such as the Mackenzie and Ob', increase by ~20% by the middle of the 21st century and by ~40% due to the quadrupling of carbon dioxide. As Manabe & Wetherald (1985) explained, the increase in discharge is attributable to the marked increase in precipitation in high latitudes, which results from the enhanced poleward transport of water vapour by daily weather disturbances (e.g. cyclone waves). The increase in poleward moisture transport is attributable mainly to the increase in absolute humidity of air in the lower troposphere, where temperature increases, particularly in high latitudes. (See Wetherald & Manabe, 2002, for a quantitative analysis of zonal mean surface water budget.) A large sensitivity of high-latitude runoff to greenhouse forcing is consistent with recent observations (Peterson *et al.*, 2002).

In low latitudes, the simulated increase in runoff is large in some regions of heavy precipitation, such as eastern Brazil and the northern Andes Mountains, northern India and the Tibetan Plateau, Indonesia, and the coastal region of Africa around the Gulf of

**Table 1** Observed (“Historical”) and simulated (“Control”) mean annual discharges ( $10^3 \text{ m}^3 \text{ s}^{-1}$ ) of major rivers of the world and relative changes simulated to occur from the pre-industrial to the middle of the 21st century (IS92a, column labelled “2050”) and in response to a quadrupling of atmospheric carbon dioxide (4×C).

River basin(s)		Mean discharge ( $10^3 \text{ m}^3 \text{ s}^{-1}$ ):		Change (%):	
		Historical	Control	2050	4×C
High Latitude	Yukon	6.5	10.1	+21%	+47%
	Mackenzie	9.1	8.5	+21%	+40%
	Yenisei	18.1	12.6	+13%	+24%
	Lena	16.9	15.1	+12%	+26%
	Ob'	12.6	6.4	+21%	+42%
	<b>Subtotal</b>	<b>63.2</b>	<b>52.7</b>	<b>+16%</b>	<b>+34%</b>
Middle Latitude	Rhein/Elbe/Weser/Meuse/Seine	3.9	3.1	+25%	+20%
	Volga	8.1	5.2	+25%	+59%
	Danube/Dnepr/Dnestr/Bug	8.5	6.7	+21%	+9%
	Columbia	5.4	6.4	+21%	+47%
	St. Lawrence/Ottawa/ Saint-Maurice/Saguenay/ Aux Outardes/Manicouagan	11.8	12.4	+6%	+12%
	Mississippi/Red	17.9	10.2	+0%	-7%
	Amur		9.2	-1%	+3%
	Huang He		16.7	+0%	+18%
	Changjiang	28.8	53.5	+4%	+28%
	Zambezi		31.1	-1%	+2%
	Paraná/Uruguay		23.5	+24%	+54%
	<b>Subtotal</b>	<b>84.4</b>	<b>97.5</b>	<b>+8%</b>	<b>+24%</b>
Low Latitude	Amazonas/Maicuru/Jari/ Tapajos/Xingu	194.3	234.3	+11%	+23%
	Orinoco	32.9	28.2	+8%	+1%
	Ganga/Brahmaputra	33.3	48.6	+18%	+49%
	Congo	40.2	122.3	+2%	-1%
	Nile	2.8	49.5	-3%	-18%
	Mekong	9.0	28.6	-6%	-6%
	Niger		58.3	+5%	+6%
	<b>Subtotal</b>	<b>312.5</b>	<b>511.5</b>	<b>+7%</b>	<b>+13%</b>
<b>TOTAL</b>	<b>460.1</b>	<b>661.7</b>	<b>+8%</b>	<b>+16%</b>	

IS92a and 4×C data are taken from Wetherald & Manabe (2002) and Manabe *et al.* (2004), respectively. The percentage change from A to B is defined as  $100 \times (B - A)/A$ . Simulated discharges have been multiplied by ratios of gauged area to simulated basin area in order to allow direct comparison, for those basins whose observations are tabulated. Subtotals and totals include only those basins with historical data. Because of insufficient computational resolution of the model, numerical results should be taken only as indicative of the potential scale of change. (The 4×C changes tabulated by Milly *et al.* (2002) for some extratropical rivers differed numerically from those tabulated here, because basin masks differed between the studies.)

Guinea (Fig. 3). As a result, the discharge from the Ganga-Brahmaputra increases by 18% by the middle of the 21st century and by 49% due to the quadrupling of carbon dioxide. The discharge from the Amazonas Rivers increases by 11% by the middle of the 21st century and by 23% in response to the quadrupling of  $\text{CO}_2$  (Table 1).

When the absolute humidity of air increases accompanying global warming, the supply of moisture to the tropical rainbelt increases, resulting in increases in precipitation and runoff over certain regions of the tropics. The relatively large percentage increase in the discharge from Ganga-Brahmaputra is attributable also to the intensifica-

tion of the Indian Summer Monsoon circulation. However, outside these regions, simulated precipitation fails to increase significantly, or decreases, thereby reducing the discharge from some tropical rivers such as the Nile and the Mekong.

In the middle latitudes, the percentage change in discharge from European and some North American rivers, such as the Volga and the Columbia, is relatively large. This response is similar to that in the high latitudes, which has already been discussed. Additionally, the change in combined discharge of the Paraná and Uruguay rivers is relatively high, reflecting essentially a tropical response within the runoff source region for this system. The change in discharge is relatively small in other mid-latitude rivers, such as the Mississippi, Zambezi and Amur. Runoff hardly changes over very extensive areas in much of the lower middle latitudes (Fig. 3).

## **SOIL MOISTURE**

A meaningful and direct comparison of modelled soil moisture with observations is not possible, because of difficulties in defining the depth of the root zone and the plant-available water-holding capacity of the soil, and because of the extreme heterogeneity of soil moisture, soil properties and vegetation rooting characteristics. In view of these difficulties, simulated soil moisture was instead evaluated on the basis of an indirect comparison. Soil moisture in this model is approximately an inverse measure of Budyko's (1974) index of dryness (Milly, 1992), which is, in turn, a strong predictor of the distribution of world biomes. Accordingly, the quality of the soil moisture was evaluated by qualitative comparison with well-known distributions of biomes.

The coupled model simulates at least qualitatively the broad-scale distribution of continental aridity (Fig. 4). For example, the regions of very low soil moisture simulated by the model correspond reasonably well with the major arid regions of the world: the Gobi and Great Indian deserts of Eurasia, North American deserts, Australian deserts, the Patagonian Desert of South America, and the Sahara and Kalahari deserts of Africa. Regions of intermediate levels of soil moisture simulated by the model correspond approximately to many semiarid regions of the world, such as the western plains of North America, the northeastern region of China, the Mediterranean coast of Europe, and the grasslands of Africa, South America and Australia.

The geographical distributions of the percentage changes in annual mean and seasonal mean soil moistures simulated for the middle of the 21st century according to the IS92a scenario are illustrated in Figs 5(a) and 6, respectively. The corresponding distributions for a quadrupling of carbon dioxide are shown in Figs 5(b) and 7. Comparing Fig. 5(a) to Fig. 5(b) and Fig. 6 to Fig. 7, one can see that, over much of the world, the response to quadrupling is substantially larger than the response in the middle of the 21st century, due to the much larger CO<sub>2</sub> increase involved. However, the overall patterns are relatively independent of the scenario.

Here the percentage change in soil moisture shown in Figs 5, 6 and 7 is described and the physical mechanism responsible for the changes is discussed. Firstly, the discussion is focused on the soil-moisture change in semiarid regions of the world, which are located in low and middle latitudes. This is followed by a brief discussion of soil-moisture change over Eurasia and North America from middle to high latitudes.

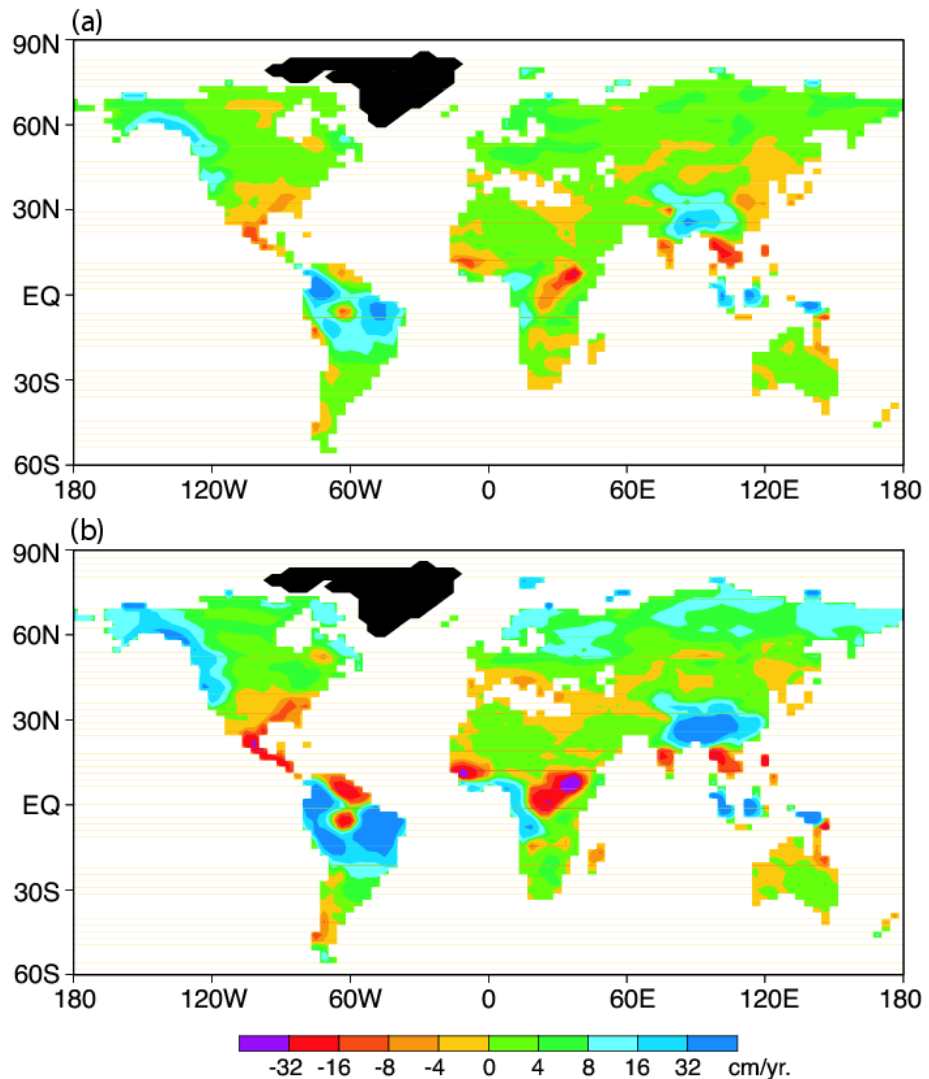


**Fig. 3** Geographical distributions of the change in the annual mean rate of runoff (cm year<sup>-1</sup>) simulated: (a) from the pre-Industrial Period to the middle of the 21st century (IS92a); and (b) in response to the quadrupling of atmospheric carbon dioxide. (a) and (b) are taken from Wetherald & Manabe (2002) and Manabe *et al.* (2004), respectively.

### Semiarid regions

Figure 5(a) and (b) indicates that annual mean soil moisture simulated by the model decreases in many semiarid regions of the world, such as the southwestern part of North America, the Mediterranean coast, the northeastern region of China, the grasslands of Africa, and the southern and western regions of Australia. The percentage reduction of soil moisture is pronounced during the dry season (Figs 6 and 7). In these semiarid regions, simulated soil moisture is reduced by a substantial fraction near the Mediterranean coast of Europe in summer (Figs 6(a) and 7(a)), in the Middle East during summer (Figs 6(a) and 7(a)) and autumn (Figs 6(b) and 7(b)), in the southern part of North America in winter (Figs 6(c) and 7(c)) and spring (Figs 6(d) and 7(d)), in South Africa in winter (Figs 6(a) and 7(a)), and in much of Australia in winter (Figs 6(a) and 7(a)) and spring (Figs 6(b) and 7(b)).

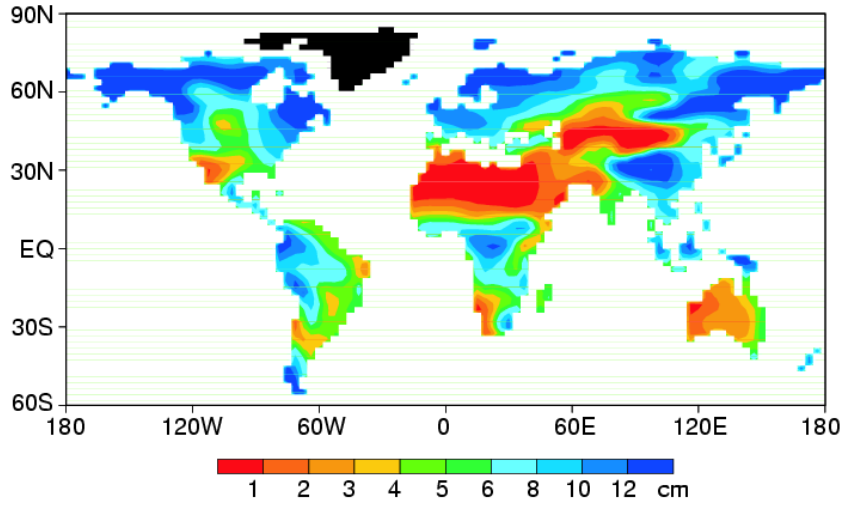


**Fig. 4** Geographical distribution of annual mean soil moisture (cm) obtained from the control experiment. From Wetherald & Manabe (2002).

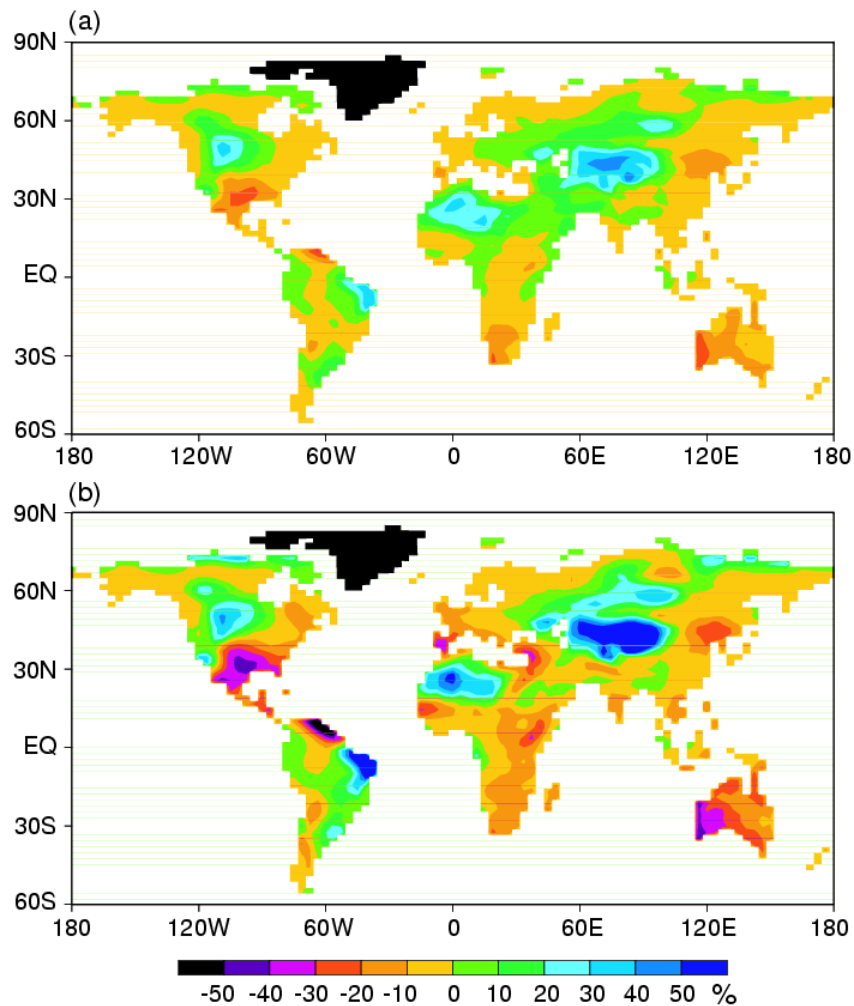


**Fig. 5** Geographical distributions of the percentage change in annual mean soil moisture simulated (a) from the pre-Industrial Period to the middle of the 21st century (IS92a) and (b) in response to the quadrupling of atmospheric carbon dioxide. The percentage change from A to B is defined as  $100 \times (B - A)/A$ . (a) and (b) are taken from Wetherald & Manabe (2002) and Manabe *et al.* (2004), respectively.

The region of relatively large soil moisture reduction (in %) is not limited to the southwestern part of North America, but extends to the southeastern part of the US (Fig. 5(a), (b)). This is attributable at least partly to poor simulation of the semiarid region in the southern part of North America. As Fig. 4 indicates, the semiarid region of relatively low soil moisture simulated by the model is not limited to the southwestern part of North America as it should be. Instead, it extends too far towards the southeastern part of North America (Fig. 4), and may be responsible for the large percentage reduction of soil moisture in the entire southern coast of the US (Fig. 5(b), (d)). If the extent of the semiarid region were simulated more realistically in the control experiment, the region with relatively large-percentage soil-moisture reduction would have been centred in the southwestern part of North America, where the actual semiarid region is located.

It is likely that a reduction of soil moisture in semiarid regions would induce the outward expansion of major deserts of the world, such as the North American desert, the Sahara and the Kalahari deserts of Africa, the Patagonian Desert of South America, and the Australian deserts (Fig. 5). A reduction of soil moisture in the northeastern region of China could induce the eastward extension of the Gobi Desert.

In the long run, soil moisture in a semiarid region seeks a level at which evaporation is equal to precipitation (Milly, 1992). As Figure 12 of the study by Wetherald & Manabe (2002) indicates, annual precipitation is reduced or fails to increase over the regions of relatively small precipitation (e.g. semiarid regions). In contrast, the annual mean rate of potential evaporation increases almost everywhere over continents as a result of the CO<sub>2</sub>-induced increase in the downward flux of infrared radiation. This is why soil moisture is reduced in semiarid regions of the world, thereby restoring the balance between precipitation and evaporation.

The reduction of precipitation in many semiarid regions of the world results from the reduction of relative humidity in the lower troposphere. As noted by Knutson & Manabe (1995), the lapse rate of temperature in a model troposphere is strongly controlled by moist convection in low latitudes and remains near the moist adiabatic value despite global warming. Therefore, the dry static stability of the troposphere increases with increasing surface temperature, thereby increasing the adiabatic heating due to the subsidence of air with a given intensity. If the overturning circulation of the troposphere in low latitudes remains approximately similar despite global warming (as noted by Knutson & Manabe, 1995), temperature becomes relatively high in regions of subsidence, thereby inducing the reduction of relative humidity. This is why precipitation is reduced over both oceanic and continental regions of relatively small precipitation, where subsidence often prevails during the dry season.

There is another factor responsible for the reduction of relative humidity over relatively arid continental regions in low latitudes. Because of low soil moisture, the increase in temperature associated with global warming is relatively large not only at the surface but also in the near-surface layer of the atmosphere, contributing to the general reduction of relative humidity in these regions.

A modelling study conducted by Rodwell & Hoskins (1996) indicates that, in summer, the increase in the heat of condensation in the Indian subcontinent generates a stationary Rossby wave pattern to the west, thereby intensifying the adiabatic descents over and around the Mediterranean Sea. The simulations carried out here indicate that, accompanying global warming, precipitation increases markedly over the Indian sub-

continent due not only to the increase in absolute humidity of air but also to the intensification of overturning circulation that results from the increase in the land–sea contrast in surface temperature. A marked increase in the Indian Summer Monsoon precipitation may be partly responsible for the reduction of relative humidity and precipitation over and around the Mediterranean Sea.

### **Summer dryness/winter wetness in middle to high latitudes**

Over very extensive regions of the Eurasian and North American continents in middle to high latitudes, the sign of soil moisture change often reverses completely between summer and winter, in contrast to the situation in semiarid regions, where it decreases during much of the year. In summer, the percentage reduction is relatively large over certain regions of Siberia and Canada (Figs 6(a) and 7(a)), whereas soil moisture increases substantially in winter in these regions (Figs 6(c) and 7(c)).

The physical mechanism responsible for the summer–winter reversal in the soil moisture change in middle and high northern latitudes was discussed in detail in preceding studies (e.g. Manabe & Wetherald, 1985; Wetherald & Manabe, 1995, 2002). Therefore, only a brief discussion is presented here, incorporating the findings gained from the present analysis. In contrast to the situation over oceans, continental surface temperature in middle and high latitudes undergoes a large seasonal variation. In winter, when surface temperature is very low in these latitudes, the increase in the downward flux of radiation due to the increase of atmospheric greenhouse gases contributes mainly to the increase of sensible heat flux rather than increase of latent heat flux of evaporation. This is why the rate of evaporation hardly increases accompanying global warming in winter. On the other hand, precipitation increases over continents due to the increase in the supply of water vapour from the oceans, where the annual variation of surface temperature is small and evaporation increases throughout the year. The increase in precipitation, in turn, results in the increase in soil moisture during winter as described above.

In summer, when surface temperature and associated saturation vapour pressure are high over continents, a major fraction of the heating due to the increase in greenhouse gases is used to enhance evaporation. In contrast, precipitation fails to increase by a similar percentage or decreases over much of Siberia and Canada, where soil is relatively dry in summer and temperature increase is relatively large not only at the surface but also in the near-surface layer of the atmosphere. The increase in temperature, in turn, induces the reduction of relative humidity and is responsible for the reduction of precipitation (or the failure to increase) despite the increase in evaporation from oceans. This is why soil moisture is reduced in summer over very extensive regions from the middle to high latitudes in the Northern Hemisphere. The timing of snowmelt in spring is another important factor responsible for the summer reduction of soil moisture. As surface temperature increases accompanying global warming, the snowmelt season ends earlier, and the soil surface, with relatively low albedo, absorbs more solar radiation. Thus, evaporation from the soil surface is enhanced, and the spring-to-summer reduction of soil moisture begins earlier, contributing to the reduction of soil moisture in the summer.

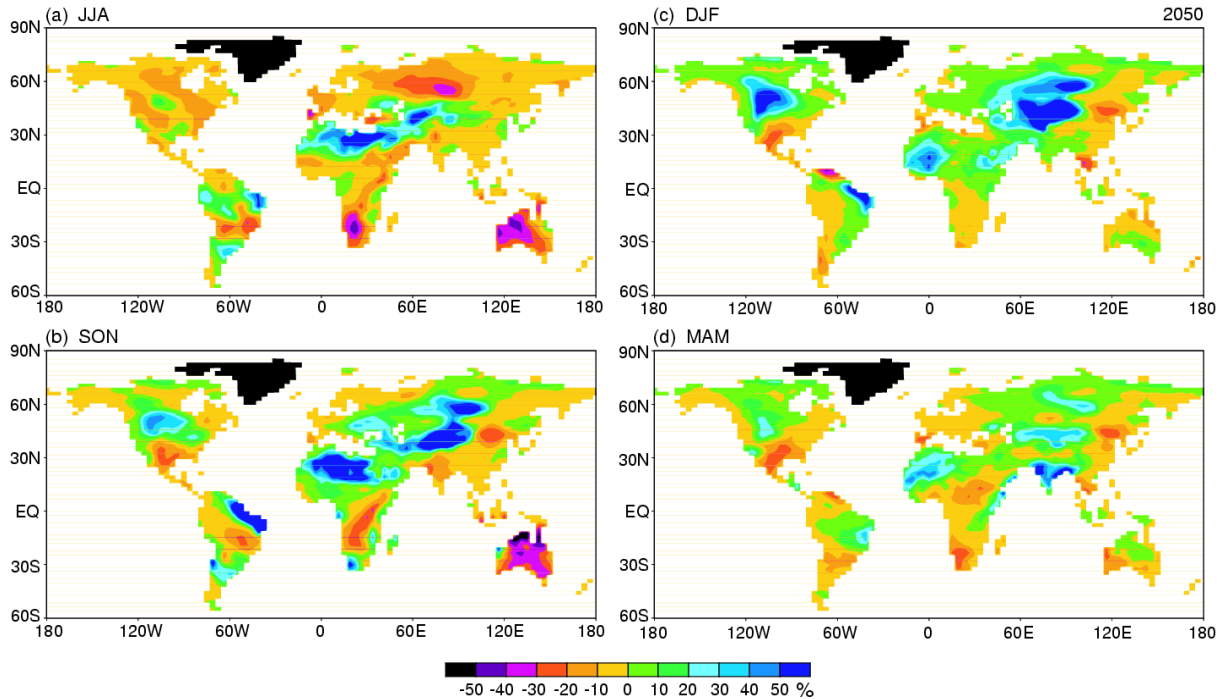


**Fig. 6** Geographical distributions of the simulated percentage changes in 3-month mean soil moistures from the pre-Industrial Period to the middle of the 21st century: (a) June-July-August (JJA); (b) September-October-November (SON); (c) December-January-February (DJF); and (d) March-April-May (MAM). See the caption of Fig. 5 for the definition of percentage change. From Wetherald & Manabe (2002).

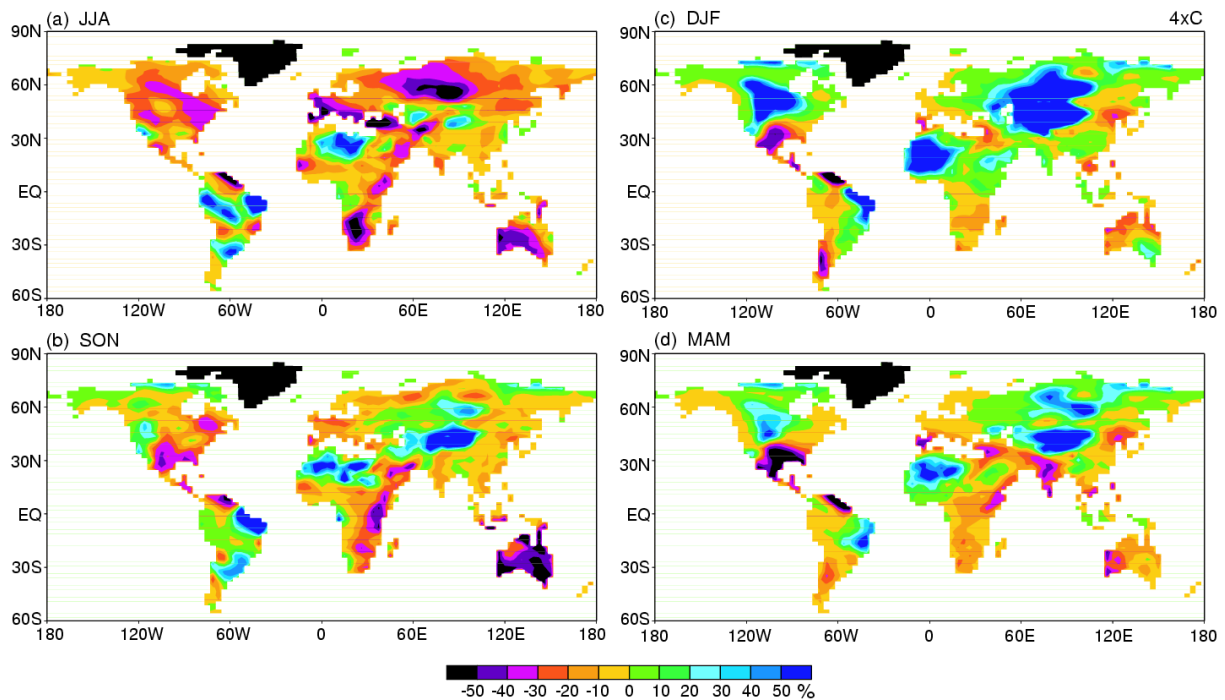


**Fig. 7** Geographical distribution of the simulated percentage change of 3-month mean soil moisture in response to the quadrupling of atmospheric carbon dioxide: (a) June-July-August (JJA); (b) September-October-November (SON); (c) December-January-February (DJF); and (d) March-April-May (MAM). See the caption of Fig. 5 for the definition of percentage change. From Manabe *et al.* (2004).

### **Very arid regions**

In contrast to the situation discussed above, simulated annual mean precipitation and soil moisture increase very slightly (but in substantial percentage) not only in winter but also in summer over some very arid regions, i.e. Central Asia and the Sahara (Figs 6 and 7). Although the specific mechanism responsible for the simulated, very slight increase in precipitation in summer was not analysed herein, a large increase in surface temperature may be responsible for enhancing very sporadic moist convective activity, thereby increasing precipitation and soil moisture over the very arid regions. Soil moisture in these very arid regions is too small to decrease further despite the increase in potential evaporation. This may be another important factor responsible for the net increase in soil moisture in very arid regions. More detailed analysis of simulated precipitation is needed to determine why simulated precipitation increases slightly, even in summer, in some of the arid regions of the world.

## **CONCLUDING REMARKS**

### **Implications for the future**

If the atmospheric concentration of carbon dioxide continues to increase, the reduction of soil moisture in many semiarid regions of the world may become increasingly noticeable during the 21st century. By the latter half of the 22nd century, when CO<sub>2</sub> concentration may quadruple, the soil-moisture change could become very substantial and almost as large as the change obtained from the CO<sub>2</sub>-quadrupling experiment. To make the matter worse, the increase in surface temperature in these regions could accelerate the evaporation from irrigated croplands, greatly increasing the demand for water. Unfortunately, runoff from these semiarid regions is not likely to increase significantly, or may actually decrease slightly, as global warming proceeds. It is therefore likely that the shortage of water in these regions will become very acute during the next few centuries. In contrast, an increasingly excessive amount of water is likely to be available in water-rich regions in high northern latitudes. The implied amplification of existing differences in water availability between different regions could present a profound challenge to the water-resources managers of the world.

### **Deficiencies in land-surface parameterization**

The results of these experiments have uncertainties associated with deficiencies in the formulation of the land parameterization. The storage of water on and below the land surface and the processes of evapotranspiration and runoff are grossly simplified in the model. Here the possible effects of parameterization deficiencies on the main results of this study are considered.

The generation of runoff is determined both by climate and by the physical characteristics of the land. In humid regions, from which the largest volumes of river discharge originate, runoff is approximately equal to the excess of precipitation over evaporative demand. In arid regions, where runoff is small, the amount of runoff is much more dependent on surface factors. However, the sensitivity of arid-land runoff to changes in climate is rather tightly constrained (Budyko, 1974). Because the funda-

mental control of the water balance by atmospheric water and energy supplies is represented in the model used in this study, it is expected that the accuracy of simulated discharge from humid and arid regions will depend mainly on the quality of simulated climate, and that shortcomings of the surface parameterization will be only of secondary importance. On this basis, it is suspected that the simulated increases in discharge in high northern latitudes and in the Ganga-Brahmaputra and Amazonas basins are robust with respect to any deficiencies in the land-surface parameterization. On the other hand, in regions of intermediate humidity (precipitation approximately equal to potential evaporation), the simplicity of our model could potentially bias the sensitivity of discharge to changes in climate.

The reasoning advanced for reliability of discharge simulations can be applied also for soil moisture, but not without a substantial qualification. The process of soil freezing, ignored in this model, undoubtedly has a strong effect on the water content of soil in cold regions. The effect is expected to be significant as long as soil frost is present in regions of seasonally frozen soil and throughout the year in permafrost regions. In warm regions, on the other hand, and particularly in the semiarid regions upon which this study focuses, the authors do not think that the large-scale pattern of the change in soil moisture would be altered substantially, had a more detailed scheme been used for representation of surface processes. Over seasonal and longer time scales, soil moisture in these regions seeks the level at which evaporation is equal to precipitation, thereby maintaining water balance (Milly, 1992). Thus, the reduction of soil moisture in these regions results from the difference between the changes in potential evaporation and precipitation. Unless a more complex model would somehow break this relationship among mean levels of precipitation, potential evaporation and soil moisture, which seems unlikely, these results for soil moisture change in warm, semiarid regions appear to be robust with respect to deficiencies in the land parameterization.

### **Comparison with other studies**

Impacts of climate change on river discharge have been estimated by use of the standalone methodology by Alcamo *et al.* (1997, 2003a,b), Arnell (1999), Vörösmarty *et al.* (2000) and Arnell (2003). Here, the focus is on the last of these, which is based upon the most recent climate simulations. The consensus pattern of change obtained by Arnell (2003) on the basis of data from several climate models (Figure 10 of his paper) is broadly consistent with the pattern obtained from the present study, with the major exception of the Amazonas River. For the Amazonas basin, Arnell (2003) finds a decrease in runoff. The difference from the result reported here arises because the consensus precipitation increase is smaller than that obtained in this model and is apparently more than offset by increases in potential evaporation.

However, differences in runoff change are not entirely attributable to differences in precipitation change scenarios. In regions of positive runoff change, such as high northern latitudes, the increase obtained by Arnell (2003) is smaller than the result presented here. In southern Europe, a region of negative change, the reduction is larger than that found here. This characterization of differences between standalone results and those reported here is true even for Arnell's (2003) results based on climate output from the model employed in the present study. Since the distribution of precipitation

change is essentially the same between the two analyses, it is likely that the difference in discharge sensitivity is mainly attributable to technical differences in the computation of potential evaporation. It appears that Arnell's (2003) changes in potential evaporation in high latitudes are generally larger than those computed in the climate simulation itself. Because Arnell computed potential evaporation using a scheme that is different from the scheme in the climate model, there is no guarantee that it satisfies the requirement of energy balance at the continental surface.

One of the critical factors that determine river discharge and soil moisture is precipitation. With the notable exception of Indochina, southern India and the coastal regions of China, the geographical pattern of simulated change in annual precipitation obtained here (shown in Figure 12 of Wetherald & Manabe, 2002) is broadly similar to that of the multi-model ensemble mean change recently obtained by IPCC (shown in Figure 9.11c of Cubasch *et al.*, 2001). For example, the multi-model precipitation from IPCC increases significantly over Siberia and Canada and decreases over many semiarid regions, in qualitative agreement with the result presented here. Quantitatively speaking, the increase in the Amazonas basin is substantially smaller than what is obtained from the present studies. The qualitative similarity between the patterns of precipitation changes obtained from the two studies suggests that the underlying physical mechanisms are similar. One should note, however, that there is a large quantitative difference among global mean precipitation changes reported by IPCC. As noted by Allen & Ingram (2002), the difference is attributable in no small part, though not exclusively, to the large inter-model difference among the changes in global mean surface temperature.

**Acknowledgements** The authors are very grateful to Thomas L. Delworth, Keith Dixon, Thomas R. Knutson and Ronald J. Stouffer, staff members of Geophysical Fluid Dynamics Laboratories of NOAA, who made the outputs from their numerical experiments available for the present study. Thomas R. Knutson and Kirsten Findell, also of the Geophysical Fluid Dynamics Laboratory, and Drs J. Alcamo, N. Arnell and T. Oki reviewed the manuscript and provided comments that were very useful for the improvement of the manuscript.

## REFERENCES

- Alcamo, J., Döll, P., Kasper, F. & Siebert, S. (1997) Global change and global scenario of water use and availability: an application of Water Gap 1.0. University of Kassel, Kassel, Germany.
- Alcamo, J., Döll, P., Henrichs, T., Kaspar, F., Lehner, B., Rösch, T., & Siebert, S. (2003a) Development and testing of the WaterGAP2 global model of water use and variability. *Hydrol. Sci. J.* **48**(3), 317–337.
- Alcamo, J., Döll, P., Henrichs, T., Kaspar, F., Lehner, B., Rösch, T., & Siebert, S. (2003b) Global estimates of water withdrawals and availability under current and future “business-as-usual” conditions. *Hydrol. Sci. J.* **48**(3), 339–348.
- Allen, M. R. & Ingram, W. J. (2002) Constraints on future changes in climate and the hydrologic cycle. *Nature* **419**, 224–232.
- Arnell, N. W. (1999) Climatic changes and global water resources. *Global Environ. Changes* **9**, S31–S49.
- Arnell, N. W. (2003) Effect of IPCC SRES\* emission scenarios on river runoff: a global perspective. *Hydrol. Earth System Sci.* **7**(5), 619–641.
- Arora, V. K. & Boer, G. J. (2001) Effect of simulated climate change on the hydrology of major river basins. *J. Geophys. Res.* **106**(D4), 3335–3348.
- Bryan, K. & Lewis L. J. (1979) A water mass model of the world oceans. *J. Geophys. Res.* **84**, 2503–2517.
- Budyko, M. I. (1974) *Climate and Life*. Academic Press, New York, USA.
- Cubasch, U., Meehl, G. A., Boer, G. J., Stouffer, R. J., Dix, M., Noda, A., Senior, C. A., Raper, S. & Yap, K. S. (2001) Projection of future climate change, Ch. 9 in: *Climate Change 2001: The Scientific Basis*, 524–582. Cambridge University Press, Cambridge, UK.

- Delworth, T. L., Stouffer, R. J., Dixon, K. W., Spelman, M. J., Knutson, T. R., Broccoli, A. J., Kushner, P. J. & Wetherald, R. T. (2002) Review of simulations of climate variability and change with the GFDL R30 coupled climate model. *Clim. Dynam.* **19**, 555–574.
- Haywood, J. M., Stouffer, R. J., Dixon, K. W., Wetherald, R. T., Manabe, S. & Ramaswamy, V. (1997) Transient response of a coupled model to estimated change in greenhouse gas and sulfate concentration. *Geophys. Res. Lett.* **24**, 1335–1338.
- IPCC (Intergovernmental Panel on Climate Change) (1992) *Climate Change 1992: The Supplementary Report to the IPCC Scientific Assessment* (ed. by J. T. Houghton, B. A. Callander & S. K. Varney). Cambridge University Press, Cambridge, UK.
- IPCC (2001) *Climate Change 2001: The Scientific Basis* (ed. by J. T. Houghton, Y. Ding, D. J. Griggs, M. Noguer, P. J. van der Linden, X. Dai, K. Maskell & C. A. Johnson). Cambridge University Press, Cambridge, UK.
- Jones, P. D. & Wigley, P. M. L. (1991) *Trend '91: A Compendium of Data on Global Change, in Global and Hemispheric Anomalies* (ed. by T. A. Boden, R. J. Spanski & F. W. Stoss), 512–515. Oak Ridge Natl Laboratory, Tennessee, USA.
- Knutson, T. R. & Manabe, S. (1995) Time-mean response over the tropical Pacific to increased CO<sub>2</sub> in a coupled ocean–atmosphere model. *J. Climate* **8**, 2181–2199.
- Manabe, S. (1969) Climate and ocean circulation: 1, The atmospheric circulation and hydrology of the Earth's surface. *Mon. Weather Rev.* **97**, 739–774.
- Manabe, S. & Wetherald, R. T. (1975) The effect of doubling the CO<sub>2</sub> concentration on the climate of a general circulation model. *J. Atmos. Sci.* **32**, 3–15.
- Manabe, S. & Wetherald, R. T. (1985) CO<sub>2</sub> and hydrology. In: *Part A. Climate Dynamics, Issues in Atmospheric and Oceanic Modeling* (ed. by B. Saltzman & S. Manabe), 131–157. Advances in Geophysics, vol. 28, Academic Press, Orlando, USA.
- Manabe, S., Smagorinsky, J. & Strickler, R. F. (1965) Simulated climatology of a general circulation model with a hydrologic cycle. *Mon. Weather Rev.* **93**, 769–798.
- Manabe, S., Stouffer, R. J., Spelman, M. J. & Bryan, K. (1991) Transient response of a coupled ocean–atmosphere model to gradual change of atmospheric CO<sub>2</sub>. Part I: Annual mean response, *J. Climate* **4**(8), 785–818.
- Manabe, S., Wetherald, R. T., Milly, P. C. D., Delworth, T. D. & Stouffer, R. J. (2004) Century-scale change in water availability: CO<sub>2</sub> quadrupling experiment. *Climatic Change* **64**, 59–76.
- Milly, P. C. D. (1992) Potential evaporation and soil moisture in general circulation models. *J. Climate* **5**, 209–226.
- Milly, P. C. D., Wetherald, R. T., Dunne, K. A. & Delworth, T. L. (2002) Increasing risk of great floods in a changing climate. *Nature* **415**, 514–517.
- Orsag, S. A. (1970). Transform method for calculating vector-coupled sums: application to the spectral form of the vorticity equation. *J. Atmos. Sci.* **27**, 890–895.
- Peterson, B. J., Holmes, R. M., McClelland, J. W., Vörösmarty, C. J., Lammers, R. B., Shiklomanov, A. I., Shiklomanov, I. A. & Rahmstorf, S. (2002) Increasing river discharge to the Arctic Ocean. *Science* **298**, 2171–2173.
- Redi, M. H. (1982) Oceanic isopycnal mixing by coordinate rotation. *J. Phys. Oceanogr.* **12**, 1154–1158.
- Rodwell, M. J. & Hoskins, B. J. (1996) Monsoon and the dynamics of deserts. *Quart. J. Roy. Met. Soc.* **122**, 1385–1404.
- Vörösmarty, C. J., Green, P., Salisbury, J. & Lammers, R. B. (2000) Global water resources: vulnerability from climate change and population growth. *Science* **289**, 284–288.
- Walker, J. C. G. & Kasting, J. F. (1992) Effect of fuel and forest conservation on future levels of atmospheric carbon dioxide. *Paleogeogr. Paleoclimatol. Paleoecol.* **97**, 151–189.
- Wetherald, R. T. & Manabe, S. (1975) The effect of changing solar constant on the climate of a general circulation model. *J. Atmos. Sci.* **32**, 2044–2059.
- Wetherald, R. T. & Manabe, S. (1995) The mechanism of summer dryness induced by greenhouse warming. *J. Climate* **8**, 3096–3108.
- Wetherald, R. T. & Manabe, S. (2002) Simulation of hydrologic changes associated with global warming. *J. Geophys. Res.* **107**, 4379–4394.

Received 24 November 2003; accepted 12 May 2004